Creep-Rupture Behavior of Weldments

Crack growth rate for a Type 308 CRE stainless steel weldment is a function of weld and base metal creep rate

BY M. J. MANJOINE

SUMMARY. Weldment strength is a function of the strengths and ductilities of the metallurgical zones of the weld geometry and the mode of loading. Weldments of the 300 series of austenitic alloys usually fail by an exhaustion of ductility in one of the zones of the weldments—that is, by a strain limit. This strain limit decreases with a lower strain rate associated with a longer rupture life and for a higher triaxiality or constraint due to geometry or loading.

Weldments can be evaluated qualitatively by the relative creep and rupture characteristics of the base and weld metal, but a quantitative evaluation requires an analysis of the weld geometry using the properties of the zones of the weldment. The analysis method should be verified by tests of weldments.

Introduction

The creep rupture properties of weldments are governed by the stress distribution with time and the damage accumulation at critical locations. The states of stress at these locations are influenced by the external loading, the geometry of the weld and component, and the dissimilar material properties of the base metal, heat affected zone, and weld metal. Thus, the weldment has a metallurgical "notch."

The elevated temperature mechanics of materials considers the effects of strain, strain rate, stress, state of stress, temperature and metallurgical state on the flow strength (Ref. 1-7) and damage accumulation (Ref. 1-3,7).

The rupture properties of welds have been determined by:

1. Testing all-weld metal samples in the directions parallel and transverse to that of the weld and comparison with those of the base metal. (Ref. 8,9,16)
2. Testing weldments containing base metal on each side of a weld (Ref. 8,9, 10,16).
3. Testing weldments in a pressure vessel or other components (Ref. 9,10, 11,16).

Weldment tests usually give more information since the geometric and metallurgical notch effects can be more closely simulated. In these latter tests the influence of residual stresses on the stress redistribution and creep strains can be evaluated (Ref. 10). Because of the complexity of the geometry and material properties, elastic-plastic creep finite element analyses have been utilized (Ref. 7, 12,13,15).

Paper sponsored by the Metal Properties Council for presentation at the 62nd AWS Annual Meeting in Cleveland, Ohio, during April 5-10, 1981.

M. J. MANJOINE is with the Westinghouse Research and Development Center, Pittsburgh, Pennsylvania.

Mechanics of Materials

Flow Stress

The flow stress under plane stress is a function of the strain, strain-rate, and temperature (Ref. 6). Typical data for a ductile alloy "D" for a constant temperature (Ref. 2) in Fig. 1 shows that the

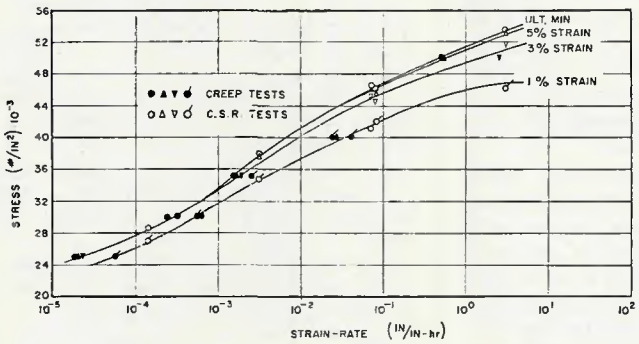

Fig. 1—Stress vs strain rate for 12Cr 3W alloy D at 1000°F (538°C)

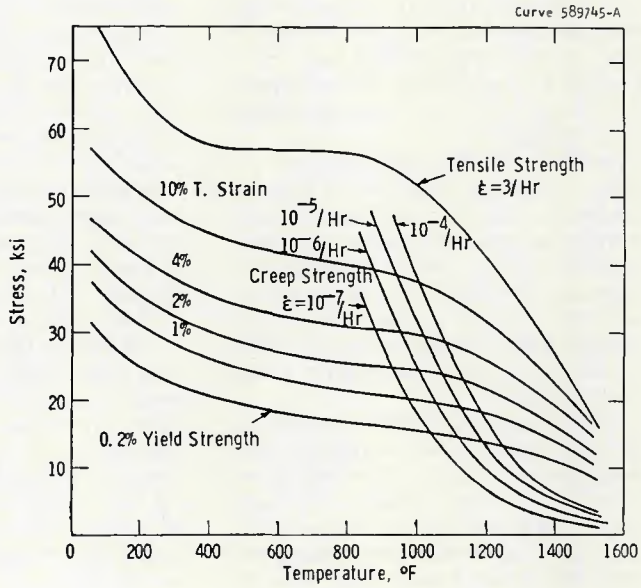

Fig. 2 (right)—Strength properties vs. temperature

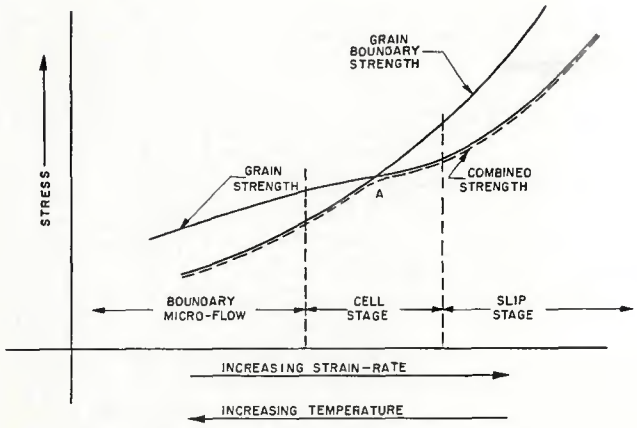

Fig. 3 — Grain and grain boundary relationship

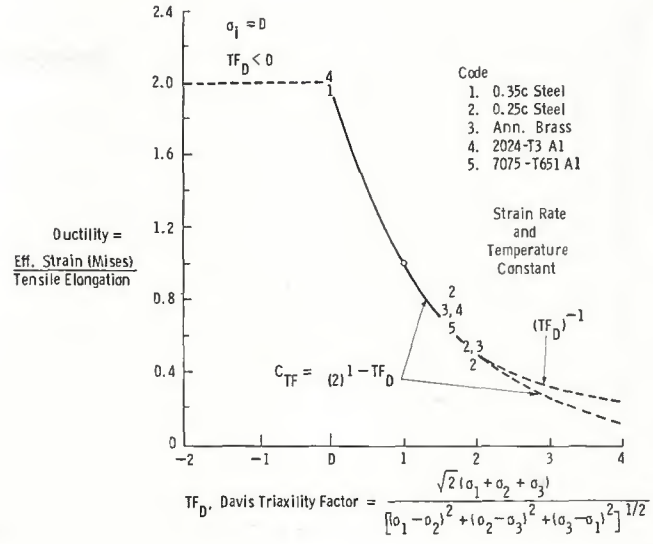

Fig. 4 (right) — Proposed ductility criteria for failure

effects of strain rate and strain can be obtained from creep or constant strain rate tests. The points for the constant strain rate data are plotted vertically and those for the creep data are plotted horizontally for the particular constant stress. Good correlation between the two types of tests was obtained for this alloy at 1000°F (538°C).

The effect of temperature on the strength of Type 304 stainless steel is illustrated in Fig. 2 for several strain rates (Ref. 6). Two sets of curves are represented:

1. Flow stress curves for 1, 2, 4 and 10% total strain and the ultimate strength, all for a strain rate of 3 per hour (h).
2. Creep strengths for minimum creep rates of 10^{-4}, 10^{-5}, 10^{-6} and 10^{-7}/h.

These curves illustrate the temperatures at which creep becomes the controlling factor in design of a component.

For the polycrystalline materials used in welded structures, flow stress and ductility are strongly dependent on the strain rate and temperature. The interrelation of these factors are dependent on the modes of flow within the grains and in the grain boundaries as shown in Fig. 3 (Ref. 2). At higher strain rates or lower temperatures, the grain strength is lower than that of the grain boundaries; in addition, the mode of flow is primarily by slip within the grains and the ductility is relatively high.

Ductility is defined as the ability of a material to flow under a given loading and redistribute stress without generating a fracture instability. This definition implies that defects or non-homogenities exist which cause local stress risers in the material. As the strain rate is decreased or the temperature raised, the strength of grain boundaries decreases more than that of the grains and a greater part of the deformation occurs in the grain boundaries. The apparent ductility is lower because of the lower volume of grain boundaries for a given critical strain and the high stress riser at boundary intersections. The boundaries are often the sites for tramp elements, precipitates, and microfissures.

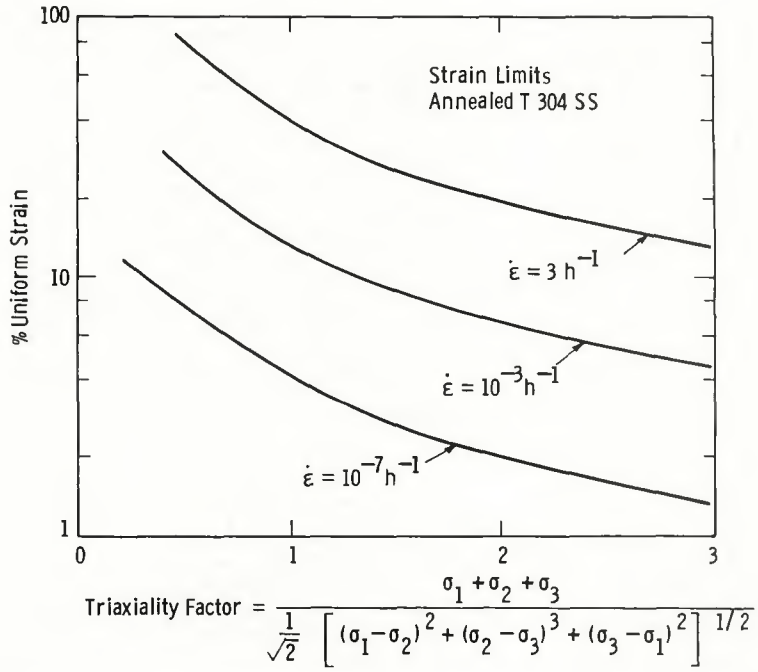

Fig. 5 — Theoretical ductility vs. triaxiality factor

Multiaxial Stress

The ductility is also a function of the state of stress because of the constraint to plastic flow. For example, under equal triaxial tension, no plastic flow can occur. From tests on ductile materials the models of ductility-ratios of Fig. 4 have been generated as a function of the triaxility factor (T.F.) equal to the sum of the principal stresses divided by the octahedral shearing stress and normalized to unity for plane stress or uniaxial tension.

For design, the lower envelope of ductility ratio is recommended. Ductility can be expressed as a function of strain rate and state of stress as shown by the curves of Fig. 5 for annealed Type 304 stainless steel at 1100°F (593°C).

The notch rupture strength ratio, based on the average axial stress of a notched bar divided by the stress for plane stress for a given life, has been used as an index of the influence of metallurgical state and state of stress. (Ref. 1,2,5,7) The notch rupture ratio for alloys A, B, C, and D are plotted as a function of notch acuity with triaxiality increasing to the left (Ref. 5).

Alloy D is the most ductile and shows increasing strength ratios greater than

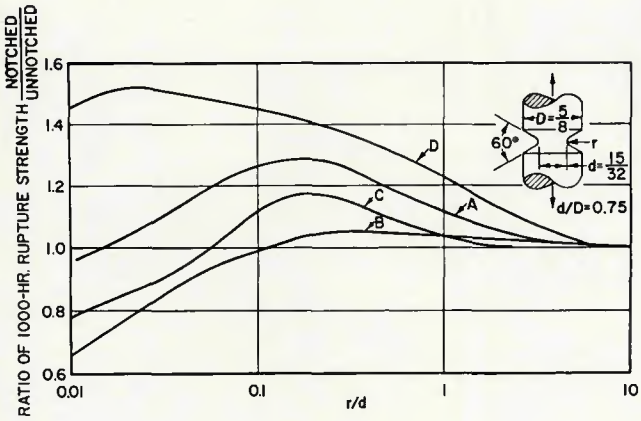

Fig. 6 – Notch rupture ratio vs. notch acuity

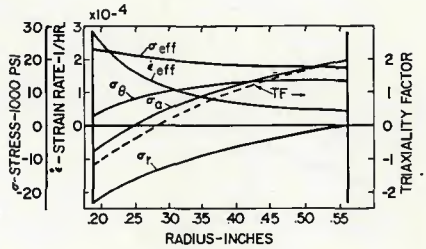

Fig. 7 – Stress distribution in thick-walled tube for biaxial tension at 1200°F (649°C)

Fig. 8 – Metallurgical zones in V-groove weld

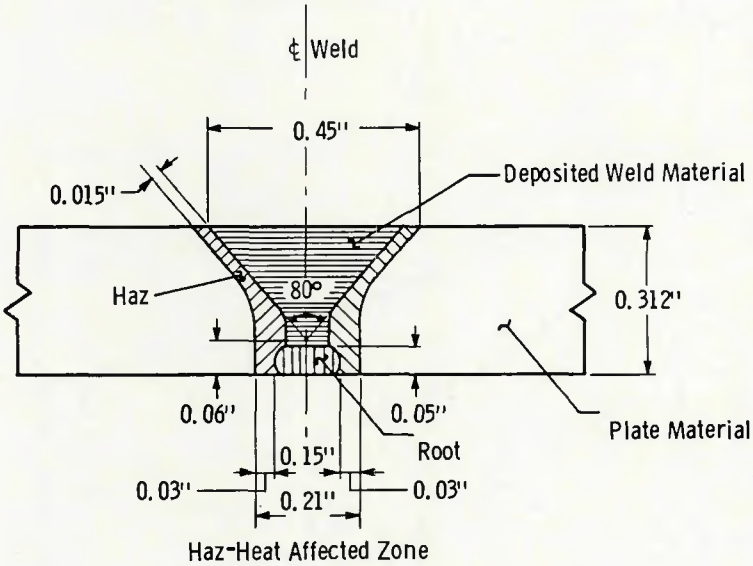

unity with increasing notch acuity. The other three are different heat treatments of an austinitic precipitation-hardened alloy and initially show increasing notch strength ratio which reaches a peak and then decreases below unity for increasing notch acuity. The notch strength ratio decreases with the decrease in ductility for the particular heat treatment under plane stress. The notch rupture ratio has also been shown to be a function of the creep characteristic for different heat treatments; the ratio is usually lower for the more creep resistant treatments especially at longer lives (Ref. 7).

Multiaxial stress is also present in thick-walled pressure vessels and pipes. For the elastic stress distribution, the maximum stress is the hoop stress at the inside diameter (I.D.). The stress distribution changes with creep and the maximum stress moves across the wall to the outside diameter (O.D.). A typical distribution of the stresses for biaxial tension after creep (Fig. 7) shows that the highest effective stress and strain are at the I.D. but the highest principal stress and triaxiality are at the O.D. (Ref. 4).

Rupture Damage

At elevated temperature and long service time, the major modes of damage under quasi-static loading are:

A. Crack initiation and growth by a maximum principal stress history,

B. Accumulation of shear strain up to a strain instability or limit.

Mode A damage is characterized by grain boundary cracks which have a direction which is "generally" perpendicular to the maximum principal stress, σ_1, where as, mode B damage exhibits granular slip and grain rotation. Combinations can also occur which interact and therefore, the total damage, D, is a function of these modes:

$$D = f\left[\Sigma\left(\frac{t_i}{t_r}\right)_{\sigma_1}, \Sigma\left(\frac{\epsilon_i}{\epsilon_L}\right)_{\dot{\epsilon},\sigma_{ij}}\right]$$

where t_i is the time increment at a given level of σ_1, and t_r is the rupture time at this stress, ϵ_i is the strain increment at a

Fig. 9 – Stress-strain characteristics of weld zones

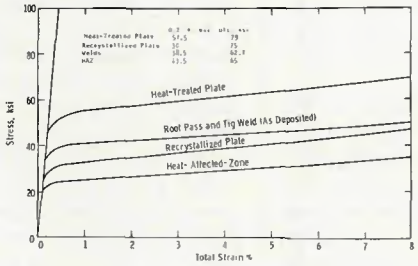

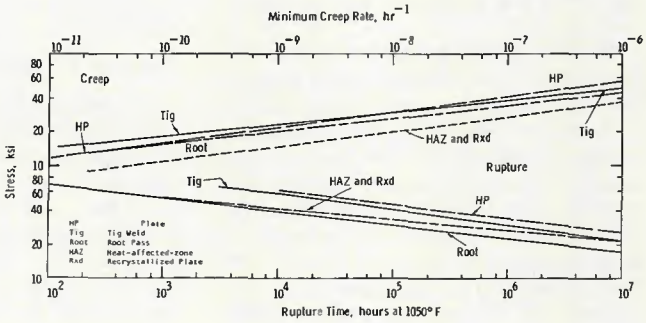

Fig. 10 – Creep-rupture properties

given strain rate, $\dot{\epsilon}$, and state of stress, σ_{ij}, and ϵ_L is the strain limit for these conditions.

The relative contribution of damage from the two modes follow the trends of Fig. 3. Mode A dominates when the grain boundary strength is weaker (low creep rates or higher temperatures) whereas Mode B dominates when the grain strength is weaker.

Stress Analysis of Weldments

The elastic-plastic-creep finite element computer method can enable an understanding of the complex stress fields in weldments under a given loading. (Ref. 3,12,13,14) Computers with high storage capacity allows the use of different materials properties for different volume of the zones of base metal, heat affected zone, root pass, and weld metal. The constitutive relations required are the tensile properties and creep-rupture properties at service temperatures for each zone.

Stress Analysis for a Circumferential "V" Groove Weld in a Pipe Under an Axial Load

The metallurgical zones in a V-groove weld are illustrated in Fig. 8. The stress-strain characteristics at service temperature of each zone were obtained from the material which had been thermally treated to simulate the welding process and are given in Fig. 9. The creep and rupture properties (Fig. 10) are shown by the upper and lower sets of curves (note the double scales) (Ref. 12).

The loading case selected for illustration of the finite element program was that which simulated an axial load on a pipe containing a transverse circumferential GTA V-groove weld through the wall (Ref. 3). The average axial stress was equal to the elastic limit of the weakest zone. The stress contours at 100,000 h for the axial stress (σ_x), the transverse or thickness stress (σ_y), and the hoop or circumferential stress (σ_z) are shown in Figs. 11–13.

The axial stress (Fig. 11) at the inside diameter decreases from the center line of the weld to the base metal (to the right). The stress gradients near the root pass illustrate the effects of the metallurgical notch. The transverse stress contours (Fig. 12) show the self-equilibrating compression and tension stresses from the constraints of the stronger base metal and the geometry of the weld. High hoop tensile stresses and gradients occur during creep because of the metallurgical notch in the pipe geometry.

On initial loading, the stresses are elastic and the stresses are uniform in all three directions. However, the nonuniform creep in the zones of the weld causes a stress redistribution (Fig. 14) and a 62% increase of the axial stress at the weld root after 100,000 h. The histories of the maximum stress in each zone are plotted in Fig. 15 and compared to the uniaxial constant stress rupture curves. The accumulative damage is greatest for the root element on the centerline of the weld. Failure is predicted at 110,000 h; this is about 50% of the desired design life — Fig. 15.

Creep and Crack Initiation of a Central Axial Weldment

A circumferential weld in a pressure vessel or pipe under internal pressure is loaded under a high degree of plane strain. The zones of the weld are constrained to have the same average hoop strain and creep rate (Ref. 10).

A specimen was designed to model a circumferential weld and a method of measuring the strain distribution was developed (Ref. 11). The specimen consisted of a Type 304 stainless steel plate with a width to thickness ratio of 10 and

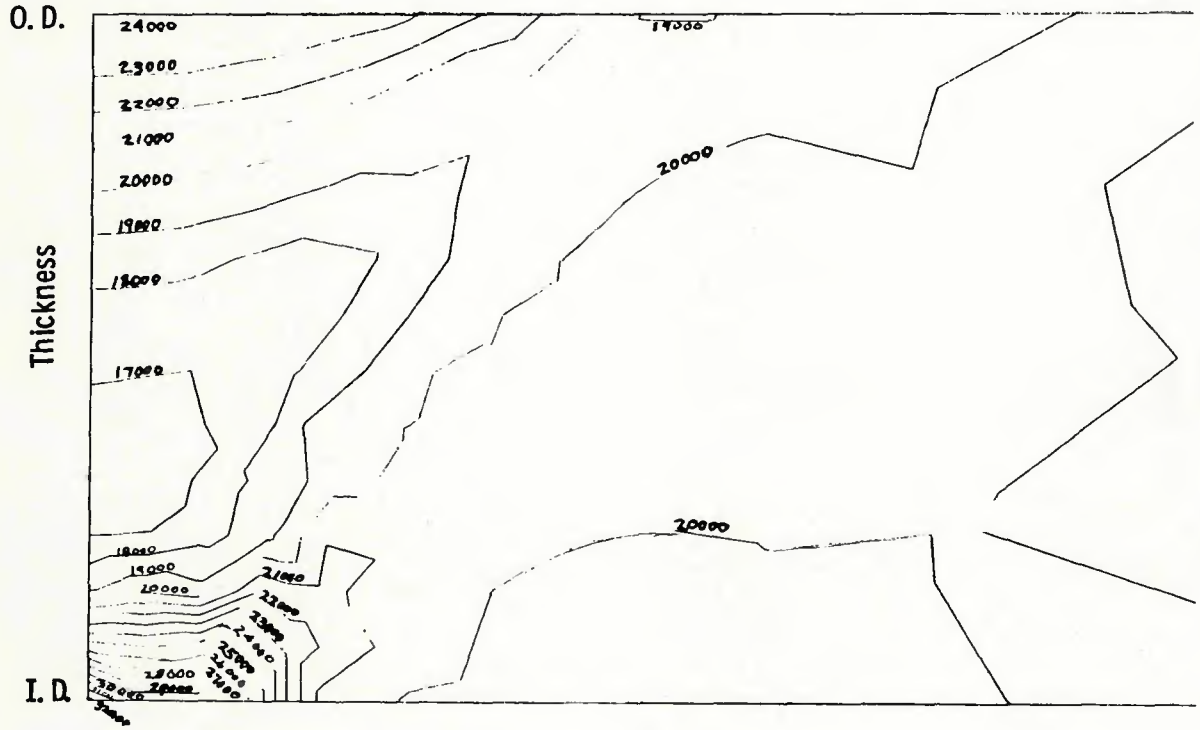

Fig. 11 — Axial stress contours, σ_x

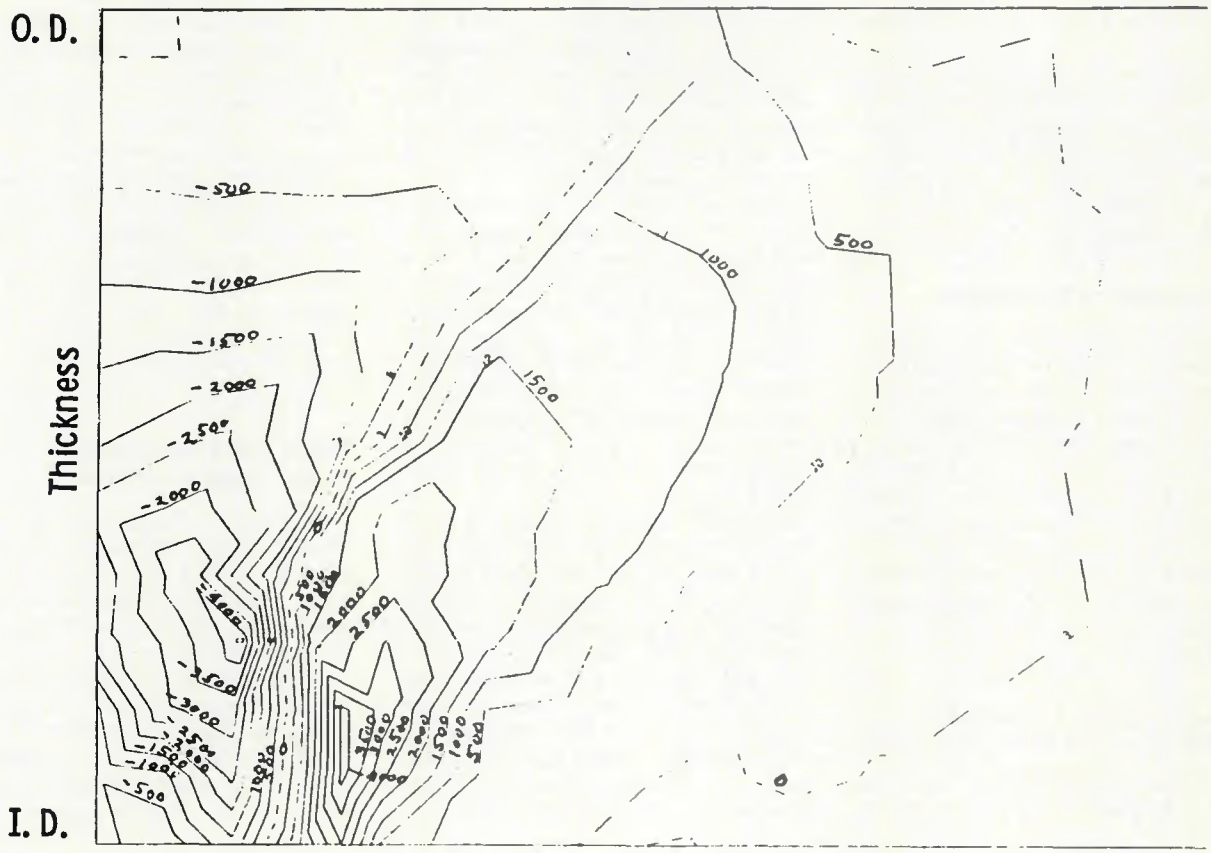

Fig. 12 — Transverse stress contours, σ_Y

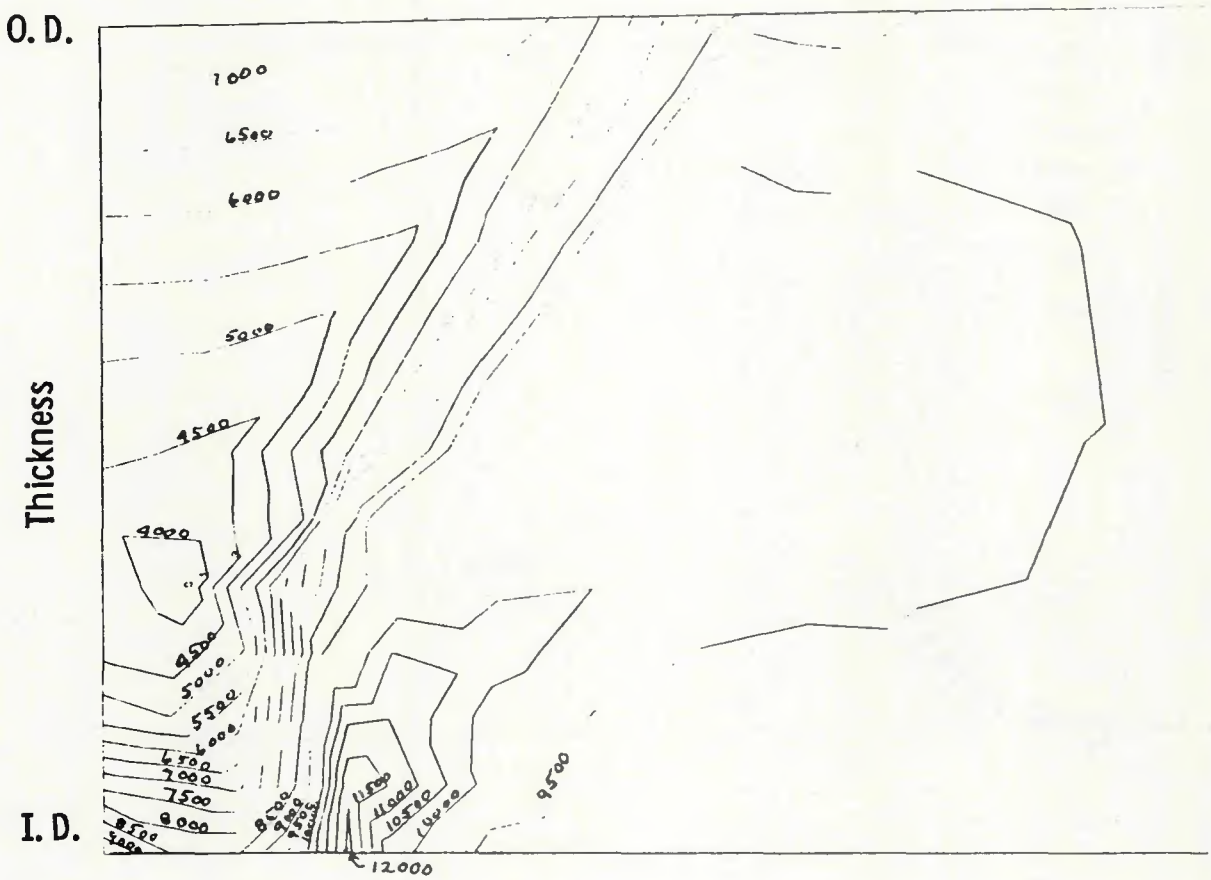

Fig. 13 — Hopp stress contours, σ_Z

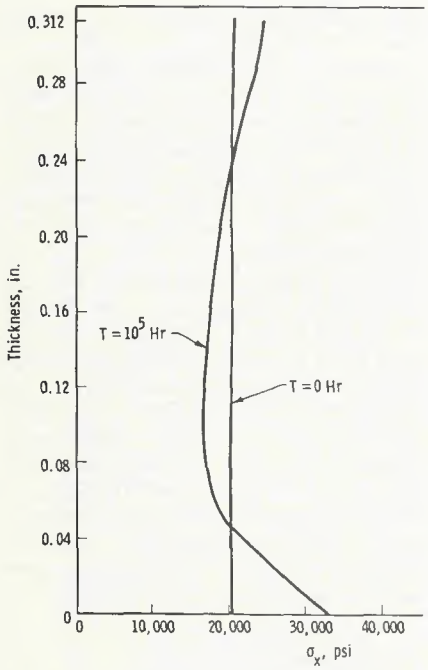

Fig. 14 — Axial stress distribution at mid-weld

containing a central axial weld of Type 308 stainless steel with controlled residual elements (CRE) (Ref. 8). The ends of the gauge section are sandwiched between heavy end plates to produce plane strain conditions. The degree of lateral constraint, however, decreases toward mid-length of the gauge section. The gauge section is marked with a square grid for strain measurements.

The weldment model was loading in the axial direction at 1100°F (593°C). The test was interrupted at intervals for gauge section measurements and to photograph the grid. Cracking initiated at about 26% of life near mid-length at the heat-affected zones (HAZ). With continued creep additional cracks initiated a short distance from the original ones. The crack pattern at 93% of life (Fig. 16) shows the major multiple initiations.

The axial strain distributions along the centerline of the weld from grid measurements (Fig. 17) illustrate that the maximum strain is near mid-length. The vertical line at 947 h indicates the location of the first crack, the two lines on subsequent distributions show the extent of cracking. The maximum creep strains and the crack length curves (Fig. 18) show that the first crack initiates at about 26% of life and grows in a near linear rate just as that of the maximum creep rate of the section at mid-length or the average overall creep rate. The crack growth rate accelerates at about 76% of life when the creep rate across the section increases.

The axial strain profiles across the width for different axial positions at 93% of life (Fig. 19) show that the strain is nearly uniform across the weld when the strains are 4% or lower for axial positions away from mid-length. Earlier in life the other axial positions were more constant across the width (Ref. 11).

The lateral strain profile across the width at 93% of life (Fig. 20) demonstrates the high lateral constraint along the length due to the rigidity at the heads. The axial strain for position 2 is 4% at the HAZ and the corresponding lateral strain is −0.64% or a ratio $\epsilon_\omega/\epsilon_a$ of −0.18.

In Fig. 21, the stress and strain ratios are plotted for a thin plate as a function of the stress ratio. For the strain ratio of $\epsilon_\omega/\epsilon_a$ of −0.18 the estimated stress ratio σ_ω/σ_a from Fig. 21 is 0.33. The triaxiality factor, T.F. is, therefore, 1.7. The strain limit from Fig. 5 for Type 304 S.S. at a creep rate of 1.4×10^{-5} per hour (.04/2886) is about 4% for a T.F. of 1.7.

Discussion

The rupture damage of weldments follow the same mechanics as other materials under multiaxial stress. The ductility decreases with decreasing strain rate and increasing triaxiality. Since the weld metal is more anisotropic and is usually composed of a number of passes, its strength and ductility shows a greater decrease with decreasing strain rate or increasing temperature. Thus the strength may be greater for short times or lower temperature, but may be less than that of the base metal for long lives or higher temperatures.

The states of stress of the zones of the weldment depend on the relative strengths of these zones and their geometry. Combinations of strain rate and temperature which result in lower grain boundary strength for the relatively highest-stressed volume damage is dominated by the maximum principal stress — Fig. 15. When the grain strength is lower, the major damage is an exhaustion of ductility or strain limit and the effective stress or maximum shear and the triaxiality are more important.

In either mode of damage the crack propagations usually follow the general direction of the maximum principal stress. In Fig. 17 the combination of strain rate, temperature, and triaxiality results in a strain limit of about 4% for the HAZ. The initial crack formed at about 26% of life. The gradient of the strain rate along the gauge section allowed multiple measurements of the strain limit with continued creep. Thus, cracks formed along the HAZ's when the creep strain reached 4%.

The regular spacing is due to the local stress redistribution when the prior crack is formed. The crack growth rate is controlled by the base metal creep rate (Fig. 18) for about 50% (26% to 76%) of the rupture life. The crack growth rate accelerated with the interaction of cracks on

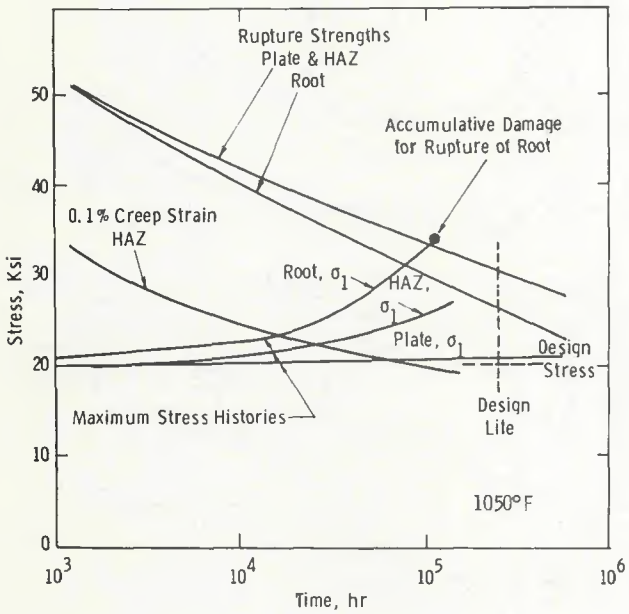

Fig. 15 (left) — Comparison of strength with stress history

Fig. 16 (below) — Cracking at heat-affected zones

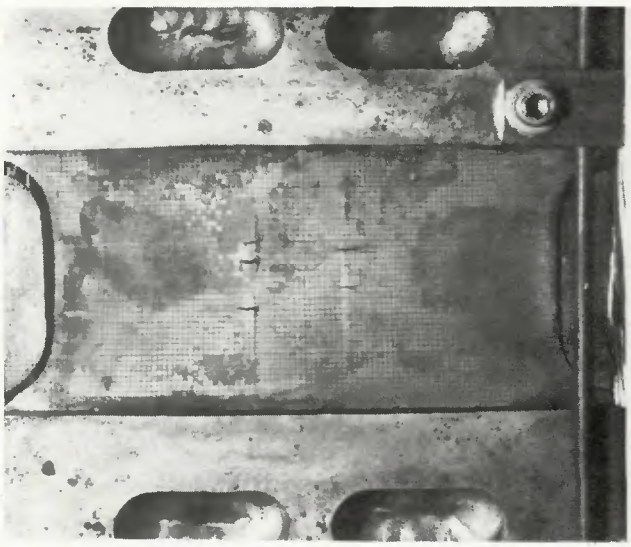

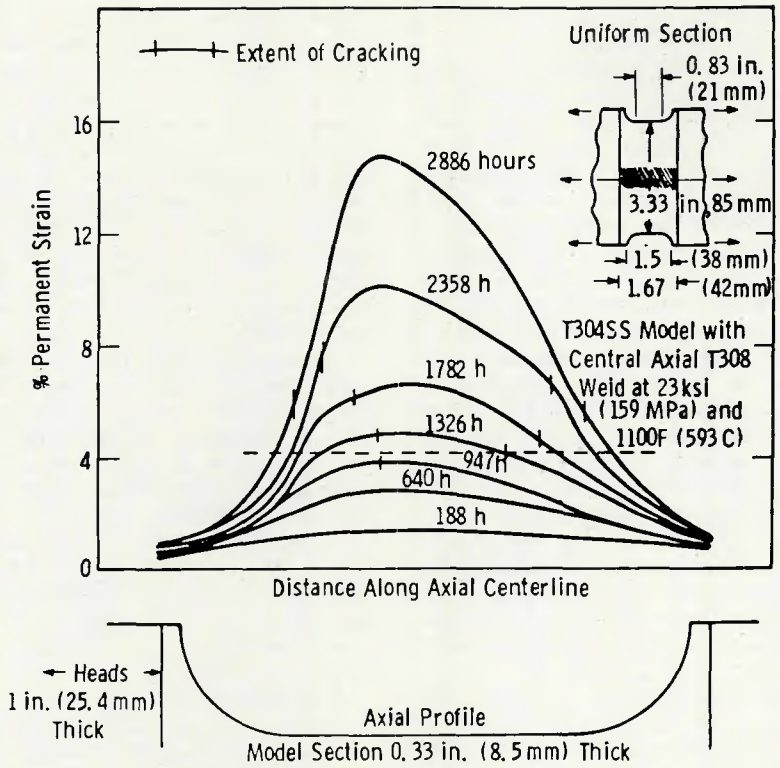

Fig. 17 — Axial strain distributions along centerline of weld

each side of the weld during the remainder of 24% of life.

Similar HAZ cracking has been reported in circumferential welds of pressure vessels (Ref. 9) where the creep strength of the weld metal was greater than that of the base metal. Weld metal cracks were also found in plate specimen with axial weld of weaker material when loading axially (Ref. 16).

The strength of weldments can be qualitatively evaluated by the relative creep and rupture characteristics of the base metal and weld metal for a direction of loading. However, a quantitative analysis requires an analysis utilizing the creep and rupture characteristics of the metallurgical zones of the weldment and their interaction. Thus, the determination of the most suitable combination of weld metal and base metal can only be obtained from weldment tests or from analyses verified by weldment tests.

Conclusions

1. The dominant damage mechanism for weldments of Type 304 stainless steel base metal with Type 308 CRE weld metal is an exhaustion of ductility. At a creep rate of 4% per 1000 h and plane strain loading parallel to the weld, trans-

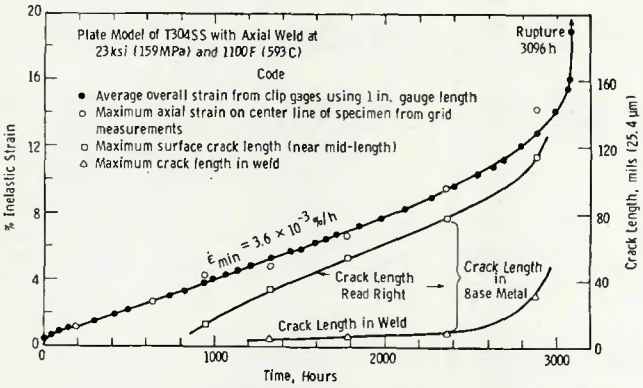

Fig. 18 — Maximum creep strains and crack length curves

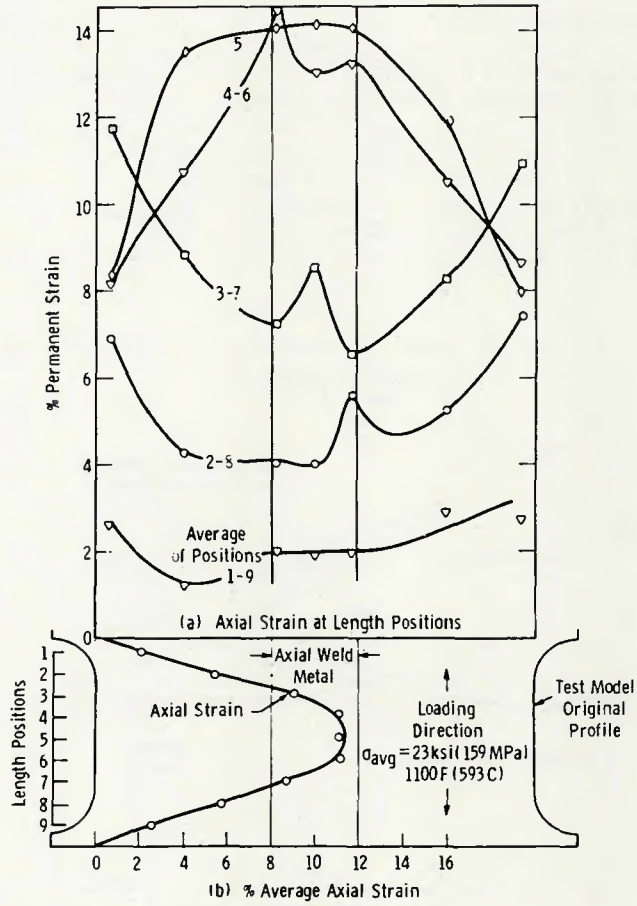

Fig. 19 — Axial strain profiles at 2886 h

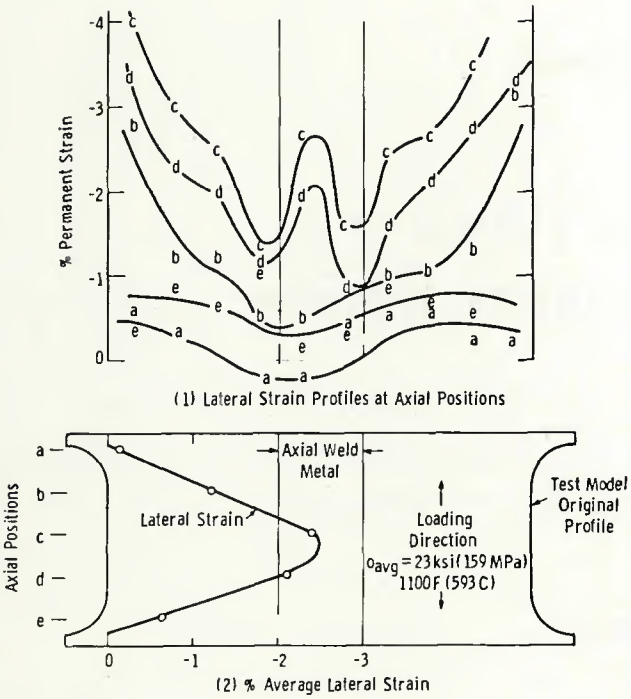

Fig. 20—Lateral strain profiles at 2886 h

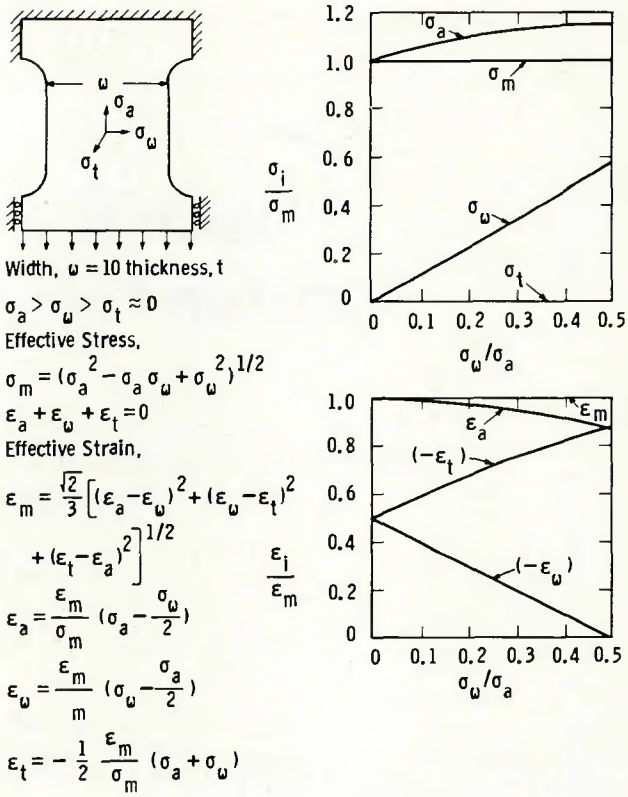

Fig. 21 (right)—Biaxial stresses and strains for plate models

verse cracking is initiated at the HAZ at 4% strain.

2. Crack growth rate for the above weldment is a function of the creep rate of the weld and base metal cross section.

3. The strength of a weldment can be qualitatively evaluated by the creep and rupture characteristics of the base metal and weld metal but a quantitative evaluation requires an analysis method which has been verified by tests of weldments.

4. The metallurgical zones of a weldment causes anisotropic creep characteristics and acts as a metallurgical notch.

5. The ductilities of the materials in the zones of the weldment decrease for lower strain rates or longer rupture lives, at higher temperatures, and at higher triaxialities or constraints.

6. When the ductility is sufficiently low, the dominant damage mechanism is crack initiation and growth for a maximum principal stress history.

References

1. Manjoine, M.J. 1975 (Apr.) Ductility indices at elevated temperatures. *ASME J. of Engineering Materials and Technology.*

2. Manjoine, M.J. 1974 Elevated temperature mechanics of metals. *1974 Symposium on Mechanical Behavior of Materials.* Kyoto, Japan.

3. Manjoine, M.J. 1971. High Temperature Stress Rupture Analysis. *Design for elevated temperature environment.* ASME.

4. Manjoine, M.J. 1970. Multiaxial stress and Fracture. *Fracture, vol. 3—Engineering Fundamentals and Environmental Effects.* New York: Academic Press.

5. Davis, E.A., and Manjoine, M.J. 1952. "Effect of notch geometry on rupture strength at elevated temperatures. *ASTM STP 128.*

6. Manjoine, M.J., 1971 (Feb.) Isochronous stress-strain curves of Type 304 stainless steel. *ASM Metals Engineering* 11 (1).

7. Taira, S., and Ohtani, R. 1974. Creep crack propagation and creep rupture of notched specimens. *Inter. conf. on creep and fatigue in elevated temperature applications.* IME.

8. King, R.T.; Stiegler, J.O.; and Goodwin, G.M. 1974. Creep properties of a Type 308 stainless steel pressure vessel weld with controlled residual elements. *Inter. Conf. on Creep and Fatigue in Elevated Temperature Applications.* IME.

9. Udoguchi, T. 1980. Recent research and developments in high temperature design in Japan. IME Proc. 194 (38).

10. Coleman, M.C., and Parker, J.D. 1981 (March). Deformation in 2CrMo-1/2 CrMoV pressure vessel weldments at elevated temperature. *Proc. inter. conf. on creep and fracture of engineering material and components.* Univ. of Swansea, (March 1981).

11. Manjoine, M.J., 1977. "Crack initiation and growth in welds at 593°C. *G1/8 SMIRT 4*

12. Chan, S.K.; Manjoine, M.J.; and Visser, C. 1971. Analyses of stresses in pressurized welded pipe in the creep range. ASME 71PVP66.

13. Walters, D.J., and R.D.H. Cockroft 1972. A stress analysis and failure criteria for high temperature butt welds. *Inter. Inst. of welding Colloquium on Creep Behavior of Welds in Boilers, Pressure Vessels and Pipelines.* Toronto.

14. Roode, F.; Etienne, C.F.; and Van Rossum, D. 1980. Stress and strain analysis for creep and plasticity of welded joints in AISI 316. *Inter. conf.—engineering aspects of creep.* Sheffield: Paper C155/118. IME.

15. Etienne, C.F.; Van Rossum, D.; and Roode, F. 1980. Creep of welded joints in AISI 316. *Inter. conf.—engineering aspects of creep.* Sheffield: Paper 155/117. IME.

16. Satok, K.; Toyoda, M.; and Satok, K. 1980. A study of creep behavior evaluation for welded joint in high temperature structure design. To be published. Denver: ASME PV&P Conf.